JACC: BASIC TO TRANSLATIONAL SCIENCE VOL. 4, NO. 4, 2019
© 2019 THE AUTHORS. PUBLISHED BY ELSEVIER ON BEHALF OF THE AMERICAN COLLEGE OF CARDIOLOGY FOUNDATION. THIS IS AN OPEN ACCESS ARTICLE UNDER THE CC BY-NC-ND LICENSE (http://creativecommons.org/licenses/by-nc-nd/4.0/).

PRECLINICAL RESEARCH

Extracellular Matrix From Hypertrophic Myocardium Provokes Impaired Twitch Dynamics in Healthy Cardiomyocytes

Lorenzo R. Sewanan, MS,[a,*] Jonas Schwan, PhD,[a,*] Jonathan Kluger, BSE,[a] Jinkyu Park, PhD,[b,e] Daniel L. Jacoby, MD,[b] Yibing Qyang, PhD,[b,c,d,e] Stuart G. Campbell, PhD[a,f]

VISUAL ABSTRACT

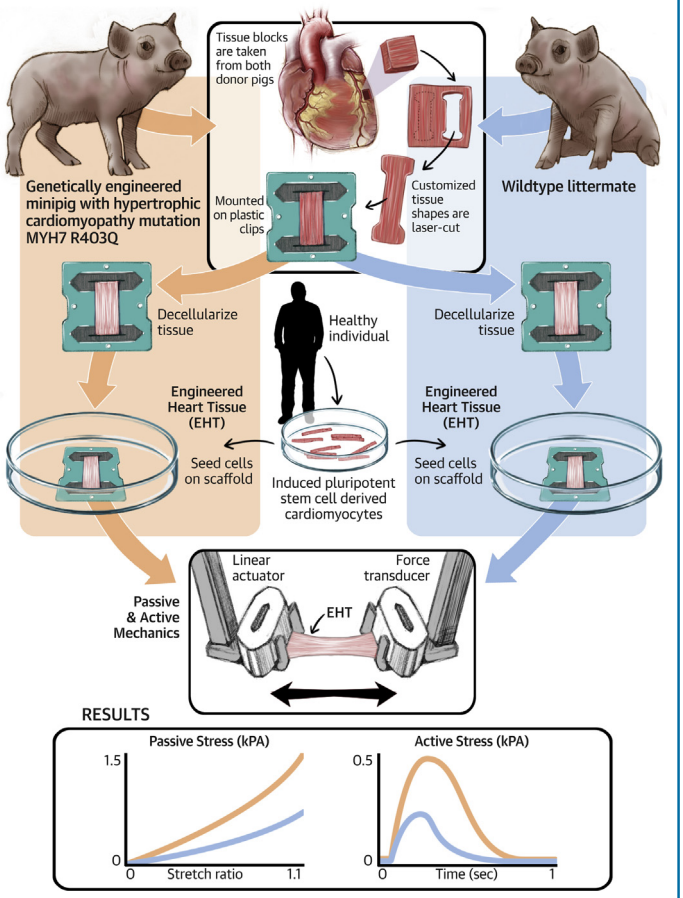

Sewanan, L.R. et al. J Am Coll Cardiol Basic Trans Science. 2019;4(4):495-505.

HIGHLIGHTS

- The goal of this study was to examine the effects of diseased extracellular matrix on the behavior of healthy heart cells.
- Myocardium was harvested from a genetically engineered miniature pig carrying the hypertrophic cardiomyopathy mutation MYH7 R403Q and from a wild-type littermate.
- Engineered heart tissues were created by seeding healthy human induced pluripotent stem cell-derived cardiomyocytes onto thin strips of decellularized porcine myocardium.
- Engineered heart tissues made from the extracellular matrix of hypertrophic cardiomyopathy hearts exhibit increased stiffness, impaired relaxation, and increased force development.
- This suggests that diseased extracellular matrix can provoke abnormal contractile behavior in otherwise healthy cardiomyocytes.

From the [a]Department of Biomedical Engineering, Yale University, New Haven, Connecticut; [b]Yale Cardiovascular Research Center, Section of Cardiovascular Medicine, Department of Internal Medicine, Yale School of Medicine, New Haven, Connecticut; [c]Yale Stem Cell Center, Yale University, New Haven, Connecticut; [d]Department of Pathology, Yale University, New Haven, Connecticut; [e]Vascular Biology and Therapeutics Program, Yale School of Medicine, New Haven, Connecticut; and the [f]Department of Cellular and Molecular Physiology, Yale School of Medicine, New Haven, Connecticut. *Mr. Sewanan and Dr. Schwan contributed equally to this work and are joint first authors. This research was supported by National Institutes of Health grants

ISSN 2452-302X https://doi.org/10.1016/j.jacbts.2019.03.004

JACC: BASIC TO TRANSLATIONAL SCIENCE VOL. 4, NO. 4, 2019
AUGUST 2019:495–505

ABBREVIATIONS AND ACRONYMS

cDNA = complementary deoxyribonucleic acid

CM = cardiomyocyte

ECM = extracellular matrix

EHT = engineered heart tissue

HCM = hypertrophic cardiomyopathy

H&E = hematoxylin and eosin

iPSC = induced pluripotent stem cell

SR = Sirius red

MTR = Masson trichrome

MUT = minipig carrying MYH7 R403Q mutation

RT50 = time from peak tension to 50% relaxation

TTP = time to peak tension

WT = wild-type

SUMMARY

Hypertrophic cardiomyopathy (HCM) is often caused by single sarcomeric gene mutations that affect muscle contraction. Pharmacological correction of mutation effects prevents but does not reverse disease in mouse models. Suspecting that diseased extracellular matrix is to blame, we obtained myocardium from a miniature swine model of HCM, decellularized thin slices of the tissue, and re-seeded them with healthy human induced pluripotent stem cell–derived cardiomyocytes. Compared with cardiomyocytes grown on healthy extracellular matrix, those grown on the diseased matrix exhibited prolonged contractions and poor relaxation. This outcome suggests that extracellular matrix abnormalities must be addressed in therapies targeting established HCM. (J Am Coll Cardiol Basic Trans Science 2019;4:495–505) © 2019 The Authors. Published by Elsevier on behalf of the American College of Cardiology Foundation. This is an open access article under the CC BY-NC-ND license (http://creativecommons.org/licenses/by-nc-nd/4.0/).

Hypertrophic cardiomyopathy (HCM) is an inherited disorder whose main clinical feature is severe left ventricular hypertrophy in the absence of elevated afterload, often leading to consequences such as diastolic heart failure, arrhythmia, and left ventricular outflow obstruction. Pathologically, HCM hearts display interstitial fibrosis and myocardial disarray (1). Decades of research into the genetic origins of HCM have identified sarcomeric gene mutations as the most common etiology (2). Such mutations have been clearly shown to alter the contractile characteristics of cardiomyocytes (CMs) (3-7), but exactly how simple contractile abnormalities lead to the diverse clinico-pathologic findings seen in HCM remains incompletely understood.

SEE PAGE 506

With the recent advent of targeted small molecule myosin modulators such as mavacamten, the possibility of preventing or even reversing HCM has emerged. Mavacamten acutely counteracts hypercontractility caused by gain-of-function HCM mutations. Studies in murine models of HCM explored the effect of myosin inhibition using mavacamten on disease development (8). As anticipated, mavacamten completely prevented hypertrophy and fibrosis in a mouse model of HCM, when administered chronically before the onset of hypertrophy. However, when the drug was introduced after the onset of measurable disease, its ability to reverse left ventricular wall thickening was limited. These findings suggest that key aspects of established HCM, including myocardial hypertrophy and perhaps even diastolic dysfunction, persist independent of the activity of the mutant protein. In other words, the pathophysiology of HCM may be self-sustaining in its more advanced stages.

One possible source of self-sustaining hypertrophic stimulus in HCM hearts is their extracellular matrix (ECM). Although the severity may vary, myocardial fibrosis is universally observed in established HCM. Evidence of abnormal ECM turnover is also seen in preclinical individuals who carry an HCM mutation (9), suggesting that ECM changes appear early and therefore could be involved in progression of the disease.

In pursuit of this hypothesis, we undertook a study of myocardial ECM obtained from a large animal model of genetic HCM (10). After histological and biomechanical characterization of myocardial samples from HCM hearts and healthy controls, we decellularized thin slices of myocardium and re-seeded them with healthy human CMs derived from an induced pluripotent stem cell (iPSC) line. By measuring the contractile behavior of these

R01 HL136590 (to Dr. Campbell) and R01 HL131940 (to Dr. Qyang), DOD 11959515 (to Dr. Qyang), an American Heart Association Predoctoral Fellowship (to Dr. Schwan), and a P.D. Soros Fellowship for New Americans (to Mr. Sewanan). Mr. Sewanan was also supported by a National Institutes of Health/National Institute of General Medical Sciences Medical Scientist Training Program Grant (T32GM007205). Drs. Schwan and Campbell have equity ownership in Propria LLC, which has licensed technology used in the research reported in this publication. This arrangement has been reviewed and approved by the Yale University Conflict of Interest Office. All other authors have reported that they have no relationships relevant to the contents of this paper to disclose. All authors attest they are in compliance with human studies committees and animal welfare regulations of the authors' institutions and Food and Drug Administration guidelines, including patient consent where appropriate. For more information, visit the *JACC: Basic to Translational Science* author instructions page.

Manuscript received December 6, 2018; revised manuscript received March 11, 2019, accepted March 13, 2019.

engineered myocardial constructs, it was possible to directly observe the effects of diseased ECM on cardiomyocyte performance and gain insights into how this factor may contribute to HCM pathophysiology.

METHODS

TISSUE HARVESTING. Flash-frozen left ventricular wall blocks from 3-month-old wild-type (WT) and mutant (R403Q) Yucatan miniature pigs (10) were provided by MyoKardia (South San Francisco, California). Breeding and tissue harvest were performed by a commercial vendor (Exemplar Genetics, Sioux Center, Iowa) and the samples shipped on dry ice. Tissues were kept frozen at -80°C until the beginning of experimental work.

HISTOLOGY. Wild-type and mutant native cardiac tissue were fixed for 24 h in 10% neutral buffered formalin (Shandon Formal-Fixx, Thermo Fisher Scientific, Waltham, Massachusetts), embedded in paraffin, sectioned at 5 μm thickness, and stained with either hematoxylin and eosin H&E. Masson trichrome (MTR), or Sirius Red (SR). Images were acquired by using 20× brightfield microscopy from multiple samples and image fields; image backgrounds were then corrected by using a 50 pixel rolling ball filter. To segment out specific features of the image, we performed color deconvolution using the ImageJ (version 1.51j8) toolbox (version 3.0.2) (11). Segmented fiber fields from MTR-stained sections and segmented nuclear fields from H&E stained sections were binarized, skeletonized, and processed by a custom MATLAB (R2017B) script (available from authors upon request), which implemented two-dimensional Fast Fourier Transform on binned and centered pixels to calculate the power distribution (12,13).

We quantified alignment as the anisotropy alignment index alpha such that $\alpha = 1 - \frac{\lambda_2}{\lambda_1}$, where the lambdas are the eigenvalues of the Cartesian fiber orientation tensor (12). To quantify the fibrosis fraction, both collagen content and total tissue content were segmented from either the MTR- or SR-stained tissue. The tissue and collagen segmentations were binarized by using the maximum entropy method in ImageJ, and the positive pixels were counted by using a custom MATLAB script; the fibrosis/tissue fraction was determined as the fraction of collagen pixels over total tissue pixels similar to published methods (14).

MAINTENANCE AND CARDIAC DIFFERENTIATION OF HUMAN iPSCs. The iPSCs used in this study were derived from T cells from a healthy adult man, previously described and extensively characterized (15). Human iPSC colonies were maintained on growth factor–reduced Matrigel (Corning, Corning, New York) at a 1:60 dilution and fed with mTESR medium every 24 h (STEMCELL Technologies, Vancouver, BC, Canada). When iPSCs reached 70% confluence, they were passaged as small colonies onto a new plate by using enzyme-free ReLeSR reagent (STEMCELL Technologies). All experiments were performed with human iPSCs between passages 35 and 45. The iPSCs were differentiated into CMs using a protocol modulating Wnt signaling as previously described (16). Briefly, after reaching ~90% confluence, iPSC colonies were treated with 17.5 μM CHIR99021 (STEMCELL Technologies) in a solution of 75% RPMI/B27-insulin and 25% mTeSR by volume. After 24 h, this culture medium was replaced with RPMI/B27-insulin. Seventy-two hours after CHIR99021 treatment, the differentiating cultures were exposed to the Wnt inhibitor IWP-4 (Tocris Bioscience, Minneapolis, Minnesota) at a concentration of 5 μM in RPMI/B27-insulin media. Media changes with RPMI/B27 (-) insulin were performed every 2 days until spontaneous beating was observed (usually between days 7 and 11 of differentiation), after which the medium was changed to RPMI/B27 (+) insulin. iPSC-CMs were used to create engineered heart tissues (EHTs) on day 14 after the start of differentiation.

EHT MANUFACTURING AND FUNCTIONAL TESTING. EHTs made out of decellularized myocardium were created similar to our previously published protocol (15). Briefly, we cut 150 μm slices from age-matched WT and mutant MYH7 R403Q porcine left ventricular blocks (MUT), which were frozen as discussed (**Figure 1A**). We omitted the sterilization process using peracetic acid and instead cultured the tissues in Dulbecco's modified Eagle medium with 10% fetal bovine serum and 2% penicillin-streptomycin overnight before seeding them the next day. For this study, we seeded both groups with exactly the same cell suspension at the same time. Active contraction mechanics were assessed as previously described (15) using a World Precision Instruments (WPI KG7) force transducer (**Figure 1B**) in Tyrode's solution at 35°C. The normalized tension-time integral was calculated as the area under the curve of the normalized twitch using numerical integration in MATLAB. To characterize intracellular calcium dynamics, some EHTs were loaded with the ratiometric fluorescent indicator Fura-2 AM (MilliporeSigma, Burlington, Massachusetts) by incubation at room temperature for 20 min in loading solution (Tyrode's solution with 17 μg/ml Fura 2-AM, 0.2% Pluronic F127, and 0.5%

FIGURE 1 Methods Used to Prepare and Test EHTs

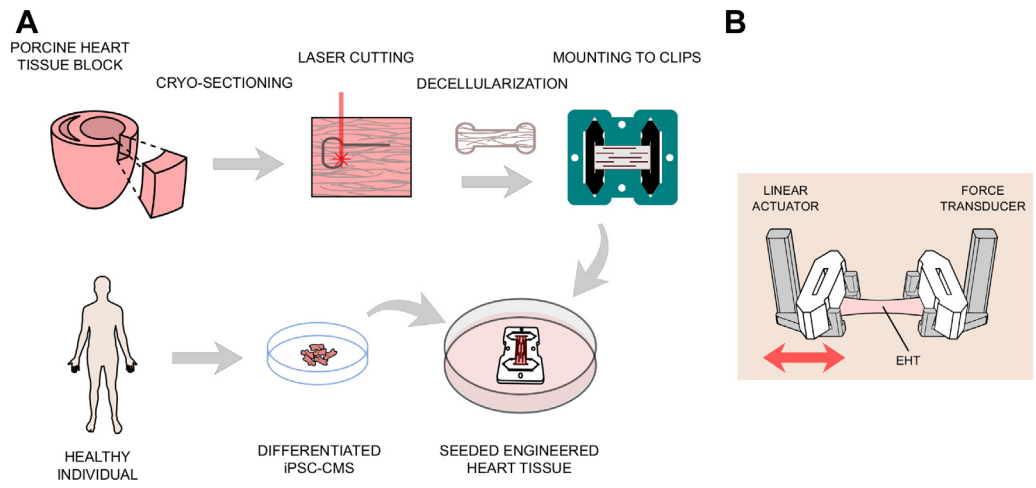

(A) Preparation of engineered heart tissues (EHTs). Tissue blocks were harvested from the left ventricular free wall and flash-frozen. Frozen blocks were sectioned into 150 μm thick slices, laser-cut into customized shapes, anchored into customized polytetrafluoroethylene (PTFE) tissue clips, and decellularized. Induced pluripotent stem cell–derived cardiomyocytes (iPSC-CMs) were seeded onto the scaffolds to create beating EHTs. **(B)** Clips were ejected out of the culturing frame and mounted on a testing setup consisting of a linear actuator and a force transducer. Force measurements were taken at different muscle lengths by moving the linear actuator.

Cremophor EL) and subsequently imaged at 35°C using a photometric system as previously described. EHTs were paced at 1 Hz during both contractile and calcium testing.

UNIAXIAL DIASTOLIC/PASSIVE MECHANICS. EHTs and tissue samples were brought to culture length (6.0 mm) on our apparatus at physiological pH (7.3) and temperature (36°C) and preconditioned for 3 cycles of 10% stretch (0.6 mm) at a rate of 0.015 mm/s (0.25% muscle length/s). After preconditioning, native and decellularized tissue from WT and MUT pig hearts were loaded and unloaded 3 times in Tyrode's solution supplemented with 20 mg/ml 2,3-butanedione monoxime (MilliporeSigma) under continuous linear stretch at a rate of 0.015 mm/s to 10% stretch. The diastolic force produced was extracted by a custom MATLAB script and normalized by cross-sectional area at culture length to calculate uniaxial tensile stress. For EHTs, a similar protocol was conducted without 2,3-butanedione monoxime.

QUANTITATIVE POLYMERASE CHAIN REACTION ANALYSIS. To analyze the gene expression patterns of EHTs generated from human iPSC-CMs, total ribonucleic acid from individual samples was extracted by using TRIzol reagent (Thermo Fisher Scientific) according to the manufacturer's instructions. Complementary deoxyribonucleic acid (cDNA) was synthesized by using an iScript cDNA synthesis Kit (Bio-Rad, Hercules, California) according to the manufacturer's instructions. Quantitative polymerase chain reaction amplifications were performed by using an IQ TM SYBR green supermix (Bio-Rad) with a total reaction volume of 15 μl, containing 1 μl of cDNA, 1.5 μl of primers, and 5 μl of distilled water, on a CFX96TM Real-Time System (Bio-Rad) using conditions of 95°C for 3 min followed by 46 amplification cycles (95°C for 10 s, 58°C for 10 s, and 72°C for 30 s). GAPDH was used as the reference gene in accordance with previous research (15). Three biological replicates were carried out for expression analysis of each gene. Primers used are listed in Supplemental Table 1.

STATISTICAL ANALYSIS. Results are given as the mean with its standard error. Statistical significance was determined by using the Student's t-test or Mann-Whitney *U* test where applicable with a confidence level of $p < 0.05$, unless stated otherwise. Calculations were conducted by using Prism 7 (GraphPad Software, La Jolla, California).

RESULTS

HISTOLOGICAL EVALUATION. Before generating EHTs from left ventricular myocardial tissue blocks from 3-month-old WT and mutant Yucatan miniature pigs, we investigated native tissue section characteristics utilizing standard histochemical stains, including H&E, MTR, and SR (**Figure 2**, Supplemental

FIGURE 2 Histological Findings in WT and MUT Porcine Extracellular Matrix

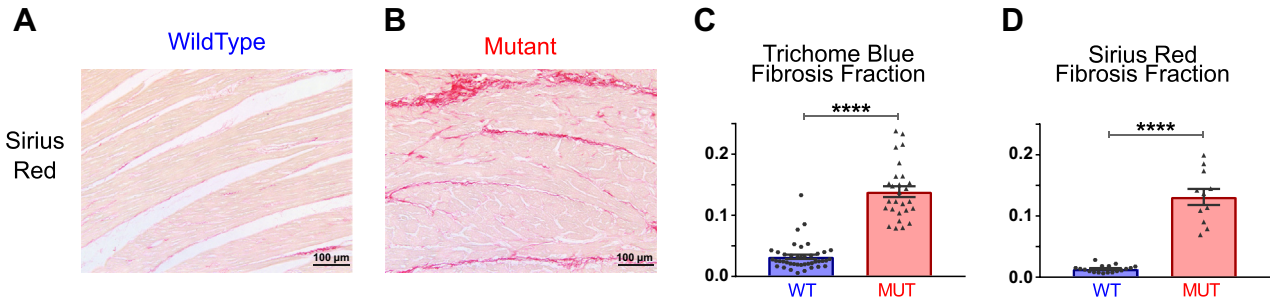

(A and B) Representative micrographs of wild-type (WT) and mutant (MUT) tissue sections stained with Sirius Red. **(C)** Masson trichrome-stained tissue showed statistically significant increase in fibrosis fraction in MUT samples (n = 27) compared with WT samples (n = 41). **(D)** Quantification of Sirius red-labeled tissue also exhibited a statistically significant increase in fibrosis fraction in MUT samples (n = 11) compared with WT samples (n = 18). ****p < 0.0001.

Figure 1). Consistent with previous microscopic findings in this large animal model (10), we observed myocyte disarray in the H&E and MTR stains and interstitial fibrosis in the MTR and SR stains, which are histopathological hallmarks of HCM (17). We further quantified the degree of disarray by image analysis of the H&E nuclear orientation and MTR fiber orientation. Significantly different alignment indexes were observed between the mutant and WT native tissue for both the nuclear alignment ($p = 0.0001$) and the fiber alignment ($p < 0.0001$); furthermore, the effect was similar for both (0.32 and 0.50, respectively), indicating a tight coupling between nuclear and fiber alignment in native cardiac tissue (18).

We quantified the degree of interstitial fibrosis and found significantly different fibrosis fraction between mutant and WT native tissues in both the MTR ($p < 0.0001$) and SR ($p < 0.0001$) stains (**Figure 2**) with a very similar average fibrosis fraction (13%) via both staining methods, indicative of moderate fibrosis (19). No overt cardiac hypertrophy was observed in these tissues; however, the occurrence of tissue remodeling and concomitant cardiac dysfunction before the development of myocardial hypertrophy and increased left ventricular wall thickness is consistent with both a previous study in this large animal model (10) and in human studies (9,20-25). We hypothesized that the moderate interstitial fibrosis and modest fiber disarray discerned through histological analysis of the mutant tissues would result in alterations of the passive properties of the mutant myocardium.

PASSIVE MECHANICS OF NATIVE TISSUE. Our EHTs allow us to perform uniaxial mechanical experiments. To determine whether the R403Q mutation leads to adverse remodeling ultimately changing uniaxial stiffness in native cardiac ECM, we used our cassette system to perform simple uniaxial characterization (**Figure 3**). In the native porcine samples (**Figure 3D**), R403Q mutant tissue exhibited an overall 3.4-fold increase in stiffness at 9% stretch (MUT [n = 3] vs. WT [n = 6], 19.6 ± 3.7 kPa vs. 5.8 ± 2 kPa; p = 0.0092) (**Figure 3E**).

PASSIVE MECHANICS OF CULTURED EHTs. Having found that native tissue of the R403Q mutant appears to be stiffer, we investigated whether decellularized tissue reseeded with iPSC-CMs maintained this property. **Figures 3A to 3C** shows typical experimental traces for 10% stretch administered to an isometrically contracting EHT (**Figure 3F**). The passive (diastolic) component of the mechanical response to stretch was obtained by examining the measured force that occurred immediately before the electrical stimulus, when the tissue was maximally relaxed. The stiffness of R403Q mutant ECM EHTs remained higher than the WT even after being seeded with healthy cells and cultured for 9 days. R403Q mutant ECM EHTs showed a 2.7-fold increased stiffness at 9% stretch (MUT EHT [n = 6] vs. WT EHT [n = 6], 21.74 ± 4.5 kPa vs. 8.05 ± 2 kPa; p = 0.0203) (**Figure 3G**). Interestingly, in 9-day-old cultured EHTs, the respective stiffness findings were similar to our native non-decellularized cardiac tissue strips; for example, non-decellularized R403Q mutant tissue had a stiffness of 19.6 kPa compared with 21.7 kPa in decellularized R403Q mutant tissue.

ACTIVE MECHANICS OF EHTs. To determine whether differences in the ECM might also alter the intrinsic contractile behavior of iPSC-CMs, we seeded tissue scaffolds of both ECM types (n = 6 each) on the same day with a homogeneous population of healthy 14-day-old iPSC-CMs. After 10 days in culture, EHTs were placed on a mechanical test apparatus and

FIGURE 3 Uniaxial Passive Mechanics of Native and Re-Cellularized Myocardial Strips

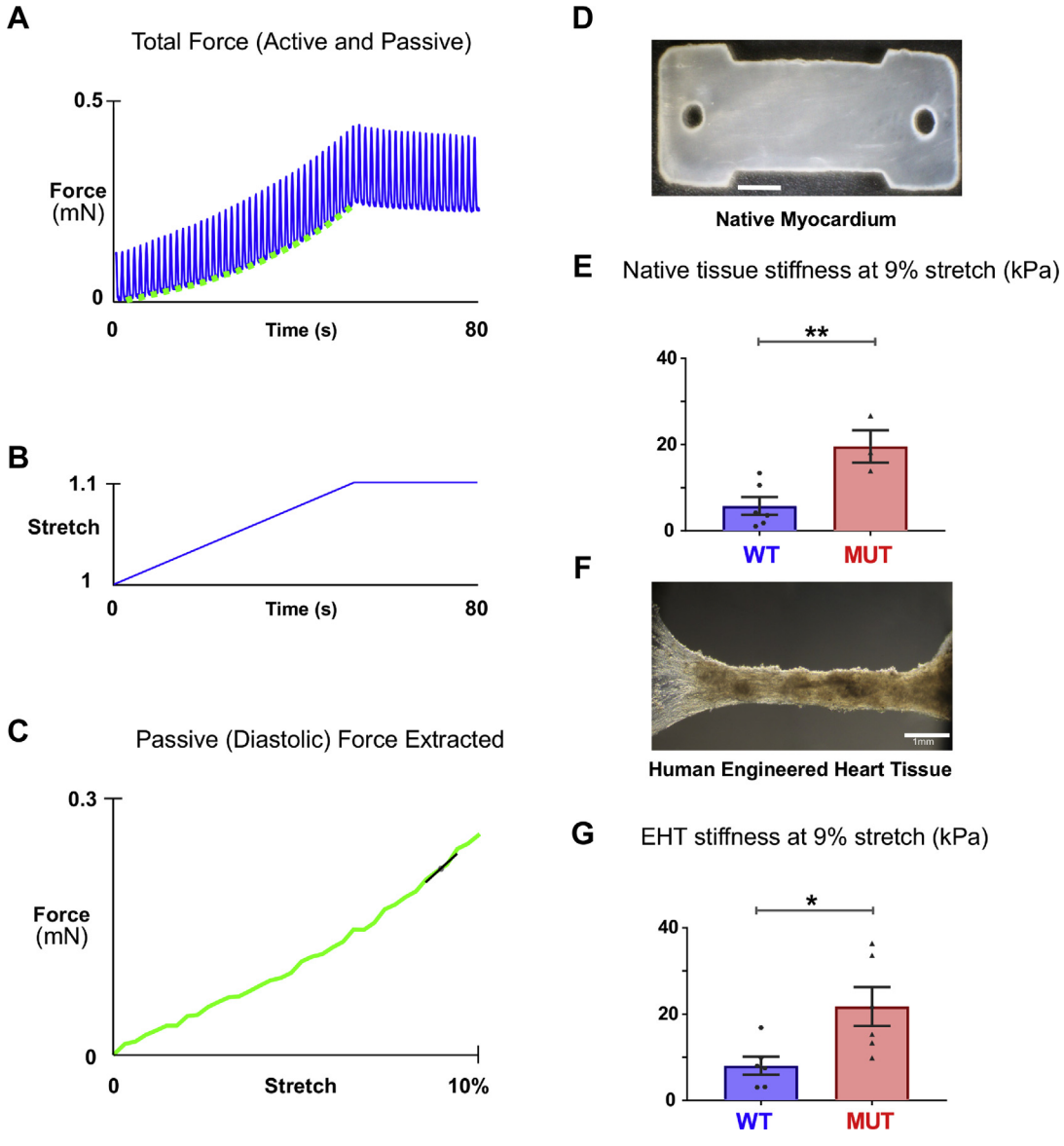

(A) Force response resulting from slow stretch of an EHT under physiological conditions paced at 1 Hz. **(B)** Tissue was uniaxially stretched at a rate of 0.25% muscle lengths per second to a final stretch of 10%. **(C)** Extracted diastolic force curve from native tissue and EHTs show the force-stretch relationship, with stiffness at 9% stretch extracted using finite difference calculation for comparison. **(D)** Typical image of a porcine myocardium laser-cut native tissue sample. **(E)** Native non-decellularized tissue stiffness of MUT samples ($n = 3$) were significantly higher than that of the WT samples ($n = 6$) ($p = 0.0092$). **(F)** Typical image of an EHT formed by re-seeding decellularized porcine myocardium with healthy iPSC-CMs. **(G)** Passive stiffness of EHTs created from MUT tissue ($n = 6$) were significantly higher than those created from WT tissue ($n = 6$) ($p = 0.0203$). *$p < 0.05$, **$p < 0.01$. Abbreviations as in Figures 1 and 2.

electrically paced at 1 Hz to capture isometric twitch force characteristics. Compared with EHTs made from healthy control ECM, R403Q mutant ECM EHTs showed prolonged early relaxation time (time from peak tension to 50% relaxation [RT50]) that was significant (190 ± 7 ms vs. 143 ± 2 ms, MUT vs. WT, respectively; $p = 0.0022$) (Figures 4A and 4B). In addition, time to peak force (TTP) was slowed significantly (262 ± 10 ms vs. 211 ± 4 ms, MUT vs. WT; $p = 0.0014$) (Figure 4C). Following on these previous observations, the normalized time tension integral was elevated in the R403Q mutant ECM EHTs

FIGURE 4 **Active Mechanics of EHTs Created From Healthy and Diseased Tissue Scaffolds**

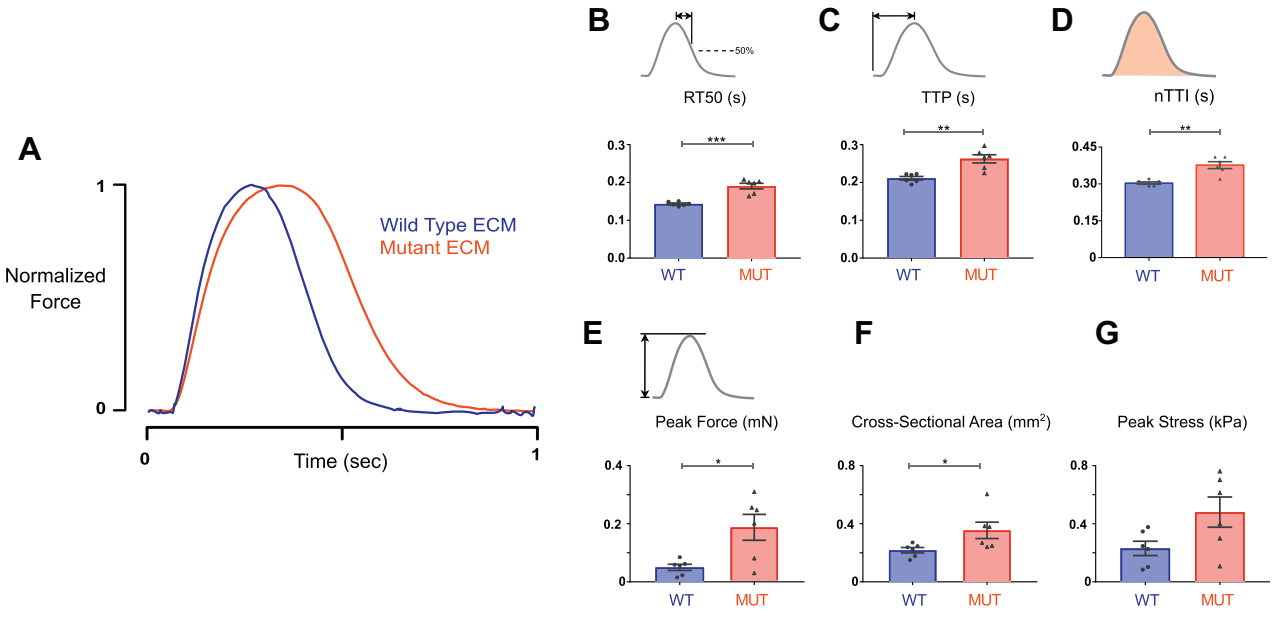

(A) Representative twitch force traces measured in EHTs created out of WT and MUT extracellular matrix (ECM). **(B)** R403Q mutant ECM EHTs showed a 33% increase in early relaxation (time from peak tension to 50% relaxation [RT50]; $p = 0.0022$). **(C)** Time to peak tension (TTP) in MUT ECM EHTs was 24% slower ($p = 0.0014$). **(D)** MUT ECM EHTs showed a 24% increase in the normalized time tension integral (nTTI; $p = 0.0043$). **(E)** Peak force was significantly increased in MUT EHTs ($p = 0.0411$). **(F)** Cross-sectional area was significantly increased in MUT EHTs ($p = 0.0411$). **(G)** Peak stress was not significantly different ($p = 0.054$). *$p < 0.05$; **$p < 0.01$; ***$p < 0.001$. Abbreviations as in Figures 1 and 2.

(0.376 ± 0.014 s vs. 0.303 ± 0.005 s, MUT vs. WT; p = 0.0043) (Figure 4D). Peak twitch force in R403Q mutant ECM EHTs was significantly higher than that of WT EHTs (0.18 ± 0.04 mN vs. 0.05 ± 0.01 mN, MUT vs. WT; p = 0.0411) (Figure 4E). Cross-sectional area differed significantly between mutant ECM EHTs and WT EHTs (0.37 ± 0.06 mm^2 vs. 0.23 ± 0.02 mm^2, MUT vs. WT; p = 0.0411) (Figure 4F). Peak twitch stress, calculated as the peak force of an EHT divided by its cross-sectional area, was not different between mutant ECM EHTs and WT EHTs (Figure 4G).

To determine whether these changes persisted beyond 10 days, we repeated EHT experiments, culturing tissues for an additional week. Differences in TTP and RT50 remained significant at this 16-day time point (Supplemental Figure 2). Furthermore, the increased contractile force in R403Q mutant ECM EHTs at 10 days remained significant at 16 days in culture.

To determine whether changes in calcium handling might account for these alterations in EHT twitch behavior, calcium transients were measured under 1 Hz electrical pacing in an independent batch of EHTs created from R403Q mutant ECM (n = 5) and WT ECM (n = 4) (Figure 5). EHTs made with mutant ECM showed a significant increase in time to peak in their calcium transients compared with EHTs made with WT ECM (0.174 ± 0.007 s vs. 0.135 ± 0.009 s, MUT vs. WT respectively; p = 0.0087). No differences were noted in other calcium transient properties, including the relaxation time constant, magnitude of calcium release, and time from peak to 80% of calcium magnitude. We further examined expression of a select panel of genes involved in HCM pathophysiology and Ca^{2+} handling, including ATP2A2, CACNA1C, TGFB2, PLN, and NPPB, using quantitative polymerase chain reaction (Supplemental Table 1). No significant differences were observed in expression of these genes between WT and MUT EHTs (Supplemental Figure 3).

DISCUSSION

To the best of our knowledge, the data presented here are the first to show the ability of diseased myocardial ECM to provoke abnormal contractile behavior in

FIGURE 5 Calcium Dynamics of EHTs Created From WT and Mutant Tissue Scaffolds

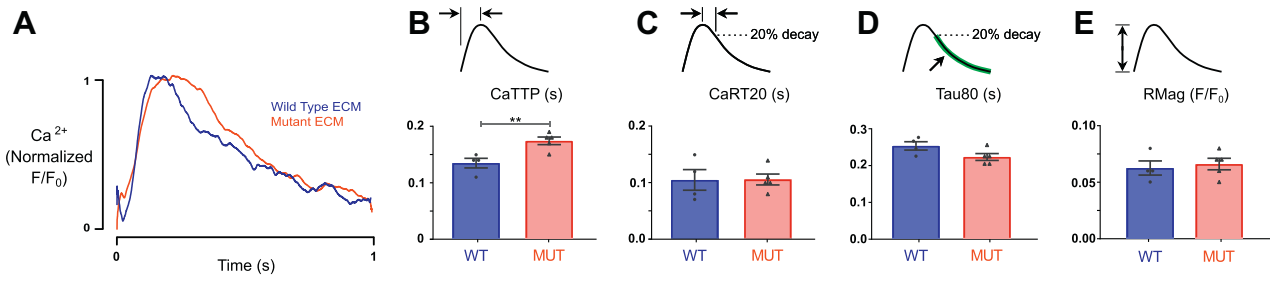

(A) Representative calcium transient traces measured in EHTs created from WT and MUT ECMs. **(B)** R403Q mutant ECM EHTs showed a 29% increase in time to peak calcium (CaTTP; $p = 0.0087$). **(C)** Time from peak to 80% calcium transient magnitude did not differ (CaRT20; $p = 0.70$). **(D)** Decay time constant from 80% peak calcium showed a trend toward being faster in the R403Q mutant ECM EHTs but did not significantly differ (Tau80; $p = 0.07$). **(E)** Peak change of calcium transient was not different (RMag; $p = 0.70$). **$p < 0.01$. Abbreviations as in Figures 1, 2, and 4.

otherwise healthy CMs, implying that ECM can store a memory of previous disease. Our findings have significant implications for understanding HCM pathogenesis and potential treatment paradigms.

It is striking that HCM ECM triggers excessive contractility and poor relaxation in CMs, because these are similar to characteristics observed in CMs expressing HCM-linked myosin mutations (26). In particular, diastolic dysfunction potentially arising from intrinsic cellular dysfunction has been increasingly recognized as a feature of HCM independent of systolic alteration and often preceding clinically significant fibrosis (27,28). Diseased ECM may have the ability to incite genetically normal cells to behave as though they harbored a sarcomeric HCM mutation. This discovery supports an intriguing hypothesis, namely that the progression of HCM is caused by a continuous cycle of mutually reinforcing phenomena: Initially, the presence of a mutant sarcomeric protein causes acute cardiomyocyte hypercontractility. This presumably triggers mechanosensitive pathways in the myocardium responsible for cellular hypertrophy and increased collagen production. As suggested by our experiments, the stiffened ECM exerts effects of its own on CMs, causing poor diastolic function and an increase in the tension-time integral. An increased tension-time integral leads to concentric hypertrophic remodeling (26,29), and the cycle repeats.

According to this paradigm, the sarcomeric mutation initiates disease but is only 1 of the factors driving disease progression in the long run. Once the secondary driver (pathological ECM remodeling) is established, removal of the sarcomeric mutation or its effects would merely diminish the disease stimulus without completely eliminating it. This viewpoint seems plausible when considering results obtained from treating mouse models of HCM with mavacamten. Green et al. (8) found that mavacamten eliminated the development of HCM pathologies in myh7 R403Q and R453C mice only when treatment began before the onset of substantial hypertrophy and fibrosis. When treatment was given after the emergence of detectable pathology, it failed to completely reverse the mechanical effects of disease, although signaling pathways leading to fibrosis were attenuated. This failure to reverse phenotype has also been shown in mouse models of HCM that feature mutations to *MYBPC3* (30). In that study, treatment with the calcium-channel blocker diltiazem was performed on 2-month-old mice with a preexisting cardiac disease phenotype. Although it had beneficial acute effects on isolated CMs, chronic treatment could not improve the tissue phenotype. The same was true for treatments with ranolazine and metoprolol (31,32).

Those studies, together with the observations presented here, offer collective insight into potential clinical treatment strategies for HCM. First, they point toward early intervention as the simplest means of preventing HCM, most easily through using targeted myosin modulators or other compounds that reduce contractility. However, in advanced HCM with significant ECM remodeling, contractile inhibition would only form part of the treatment paradigm; a secondary agent modifying the fibrotic environment described in our experiments will likely be required as well. Given the difficulty and complexity of multimodal therapy for advanced HCM, preventative therapy in patients with subclinical HCM and carriers would likely be a more fruitful approach.

The importance of fibrosis in the development of HCM is supported by numerous studies. Patients with HCM can exhibit diastolic dysfunction along with myocardial collagen deposition at early stages of the disease even when overt hypertrophy has not yet been observed (33), suggesting that subclinical fibrosis may not be merely a secondary effect but an important contributor to disease development. Indeed, one study reported an elevation of myocardial collagen content by 72% in patients with HCM compared with other hearts that had hypertrophied due to other reasons (34). A second study found that young patients with HCM and sudden death had an 8-fold increase in myocardial collagen fraction compared with control subjects and a 3-fold increase compared with patients with systemic hypertension (35). These findings are supported by the fact that systemic collagen I synthesis seems to be elevated in patients with both early and established HCM (9,36). The present study adds a new dimension of importance to fibrosis in HCM by showing a clear link between systolic contractile behavior of CMs and the supposedly "passive" mechanical characteristics of diseased ECM. Further study of the mechanisms that constitute the ECM–contractility axis is likely to yield novel therapeutic targets for disrupting and reversing established HCM.

Given the stark difference in matrix stiffness between HCM and control hearts, the observed contractility differences are not entirely surprising (37,38). The prolonged calcium transients that we observed in EHTs made from mutant ECM could easily account for the accompanying prolongation of twitch contractions. Aside from affecting contractile dynamics, ECM-mediated prolongation of the calcium transient could be a substrate for arrhythmias in HCM. Prolonged calcium transients have been linked to arrhythmogenic behavior in models of long QT syndrome (39) and sarcomeric HCM (40–42).

Changes in cardiomyocyte calcium handling have been reported before in studies in which substrate stiffness is altered in simplified biomaterial matrices and then seeded with neonatal rat CMs (38,43–45). These studies found either an increase in calcium transient duration or magnitude in response to increased substrate stiffness, at least up to a point. Extreme stiffness leads to decreased calcium transient duration and magnitude (38,44,46). Importantly, changes in calcium transient and altered contractility have also been observed in adult rat CMs grown on substrates of different stiffness (47), indicating that neonatal and adult CMs have a significant adaptive response to different mechanical environments.

Despite multiple reports linking substrate stiffness and cardiomyocyte phenotypes, the underlying mechanisms responsible remain incompletely understood. Nevertheless, stiffness-mediated changes in calcium transients have been correlated with SERCA2a expression, L-type calcium current, and action potential morphology in other studies (38,46). In the present study, we assessed expression of key calcium handling genes (ATP2A2, CACNA1C, and PLN), but these levels were unaltered in cells grown on the R403Q mutant ECM. This outcome suggests that mutant ECM provokes a response in CMs which differs from responses triggered by changes in substrate stiffness alone.

Even as these simple experiments have established an interesting relationship between myocyte contractility and diseased myocardial ECM, much remains to be determined. For instance, it is unclear whether ECM stiffness alone is sufficient to account for the observed effects. Healthy and mutation-produced matrices may also show differences in composition that go beyond ECM collagen fraction, orientation, and stiffness. Future research will explore experimental approaches for investigating matrix composition, cellular responses, and cellular mechanotransduction pathways in the context of HCM-derived ECM.

STUDY LIMITATIONS. Limitations of the artificial tissue system used to perform these initial studies should also be recognized. Our approach necessarily includes differences with native tissue; whereas native tissue consists of CMs and fibroblasts supplied by a dense capillary bed, our model system is avascular and lacks endothelial cells. Our experimental system has the advantage of allowing the introduction of CMs directly into mature matrix from any source, although this approach differs from the developmental process of native tissue, which produces and remodels ECM gradually over time. In terms of contractile behavior, EHTs created from WT myocardial ECM display twitch time-course characteristics that match those measured in isolated adult human trabeculae to well within the bounds of experimental uncertainty. Specifically, the WT EHTs exhibited mean TTP and RT50 values of 211 ms and 143 ms, compared with values of 219.3 $\pm$ 15.0 ms and 142.4 $\pm$ 11.4 ms, respectively, in isolated adult human trabeculae (48,49). We see this finding as confirming the relevance of kinetic changes observed in MUT EHTs. However, the peak active contractile stress

produced by EHTs in this study (0.23 kPa) is only a fraction of that measured in native human myocardium (~20 kPa). Differences between native and engineered myocardium suggest that complementary in vivo approaches should be developed to further probe the role of ECM remodeling in the progression and maintenance of HCM disease phenotypes.

CONCLUSIONS

Our research provides evidence that altered ECM might be a major player in the pathology and pathogenicity of HCM. The diseased ECM seems to push healthy CMs toward contractile characteristics reminiscent of those caused by HCM-linked sarcomeric mutations. Hence, contractile abnormalities in HCM may originate in sarcomeric proteins and worsen in advanced disease through the indirect influence of pathologically remodeled ECM. From a clinical standpoint, this finding suggests the importance of addressing ECM changes in any strategy for treating established HCM.

ACKNOWLEDGMENTS The authors thank Viet Dau for his assistance with imaging histological slides. Tissue samples were generously donated by MyoKardia (Dr. Sarah MacInnes).

ADDRESS FOR CORRESPONDENCE: Dr. Stuart G. Campbell, Department of Biomedical Engineering, Yale University, 55 Prospect Street, MEC 211, New Haven, Connecticut 06511. E-mail: stuart.campbell@yale.edu.

PERSPECTIVES

COMPETENCY IN MEDICAL KNOWLEDGE: Sarcomeric mutations leading to HCM alter contractile behavior and have recently become a target for treatment. Often when HCM has manifested clinically, significant remodeling of the ECM such as interstitial fibrosis has occurred. ECM remodeling likely serves to sustain and exacerbate disease phenotypes such as diastolic dysfunction.

TRANSLATIONAL OUTLOOK: Myosin modulator-dependent reversal of HCM disease expression is attenuated by ECM abnormalities once development of clinically significant hypertrophy has occurred. Future research should investigate modalities to reverse ECM remodeling to treat established HCM.

REFERENCES

1. Marian AJ, Braunwald E. Hypertrophic cardiomyopathy: genetics, pathogenesis, clinical manifestations, diagnosis, and therapy. Circ Res 2017;121:749–70.

2. Alfares AA, Kelly MA, McDermott G, et al. Results of clinical genetic testing of 2,912 probands with hypertrophic cardiomyopathy: expanded panels offer limited additional sensitivity. Genet Med 2015;17:319.

3. Ferrantini C, Coppini R, Pioner JM, et al. Pathogenesis of hypertrophic cardiomyopathy is mutation rather than disease specific: a comparison of the cardiac troponin T E163R and R92Q mouse models. J Am Heart Assoc 2017;6. pii.e005407.

4. Chuan P, Sivaramakrishnan S, Ashley EA, Spudich JA. Cell-intrinsic functional effects of the α-cardiac myosin Arg-403-Gln mutation in familial hypertrophic cardiomyopathy. Biophys J 2012;102:2782–90.

5. Viswanathan MC, Schmidt W, Rynkiewicz MJ, et al. Distortion of the actin A-triad results in contractile disinhibition and cardiomyopathy. Cell Rep 2017;20:2612–25.

6. Michele DE, Coutu P, Metzger JM. Divergent abnormal muscle relaxation by hypertrophic cardiomyopathy and nemaline myopathy mutant tropomyosins. Physiol Genomics 2002;9:103–11.

7. Fraysse B, Weinberger F, Bardswell SC, et al. Increased myofilament Ca2+ sensitivity and diastolic dysfunction as early consequences of Mybpc3 mutation in heterozygous knock-in mice. J Mol Cell Cardiol 2012;52:1299–307.

8. Green EM, Wakimoto H, Anderson RL, et al. A small-molecule inhibitor of sarcomere contractility suppresses hypertrophic cardiomyopathy in mice. Science 2016;351:617–21.

9. Ho CY, López B, Coelho-Filho OR, et al. Myocardial fibrosis as an early manifestation of hypertrophic cardiomyopathy. N Engl J Med 2010;363:552–63.

10. del Rio CL, Henze MP, Wong FL, et al. A novel mini-pig genetic model of hypertrophic cardiomyopathy: altered myofilament dynamics, hyper-contractility, and impaired systolic/diastolic functional reserve in vivo. Circulation 2018;136. Abstract 20770.

11. Schneider CA, Rasband WS, Eliceiri KW. NIH image to ImageJ: 25 years of image analysis. Nat Methods 2012;9:671–5.

12. Ayres C, Bowlin GL, Henderson SC, et al. Modulation of anisotropy in electrospun tissue-engineering scaffolds: analysis of fiber alignment by the fast Fourier transform. Biomaterials 2006;27:5524–34.

13. Sander EA, Barocas VH. Comparison of 2D fiber network orientation measurement methods. J Biomed Mater Res A 2009;88:322–31.

14. Hadi AM, Mouchaers KTB, Schalij I, et al. Rapid quantification of myocardial fibrosis: a new macro-based automated analysis. Cell Oncol 2011;34:343–54.

15. Schwan J, Kwaczala AT, Ryan TJ, et al. Anisotropic engineered heart tissue made from laser-cut decellularized myocardium. Sci Rep 2016;6:32068.

16. Lian X, Zhang J, Azarin SM, et al. Directed cardiomyocyte differentiation from human pluripotent stem cells by modulating Wnt/β-catenin signaling under fully defined conditions. Nat Protoc 2013;8:162–75.

17. Hughes SE. The pathology of hypertrophic cardiomyopathy. Histopathology 2004;44:412–27.

18. Zach B, Hofer E, Asslaber M, Ahammer H. Automated texture analysis and determination of fibre orientation of heart tissue: a morphometric study. PLoS One 2016;11:e0160735.

19. White SK, Sado DM, Fontana M, et al. T1 mapping for myocardial extracellular volume measurement by CMR. J Am Coll Cardiol Img 2013;6:955–62.

20. Germans T, Wilde AAM, Dijkmans PA, et al. Structural abnormalities of the inferoseptal left ventricular wall detected by cardiac magnetic resonance imaging in carriers of hypertrophic cardiomyopathy mutations. J Am Coll Cardiol 2006;48:2518–23.

21. Ho CY, Day SM, Colan SD, et al. The burden of early phenotypes and the influence of wall

thickness in hypertrophic cardiomyopathy mutation carriers: findings from the HCMNet study. JAMA Cardiol 2017;2:419–28.

22. Yiu KH, Atsma DE, Delgado V, et al. Myocardial structural alteration and systolic dysfunction in preclinical hypertrophic cardiomyopathy mutation carriers. PLoS One 2012;7:e36115.

23. Germans T, Rüssel IK, Götte MJW, et al. How do hypertrophic cardiomyopathy mutations affect myocardial function in carriers with normal wall thickness? Assessment with cardiovascular magnetic resonance. J Cardiovasc Magn Reson 2010; 12:13.

24. Noureldin RA, Liu S, Nacif MS, et al. The diagnosis of hypertrophic cardiomyopathy by cardiovascular magnetic resonance. J Cardiovasc Magn Reson 2012;14:17.

25. Rüssel IK, Brouwer WP, Germans T, et al. Increased left ventricular torsion in hypertrophic cardiomyopathy mutation carriers with normal wall thickness. J Cardiovasc Magn Reson 2011;13: 3.

26. Davis J, Davis LC, Correll RN, et al. A tension-based model distinguishes hypertrophic versus dilated cardiomyopathy. Cell 2016;165:1147–59.

27. Coppini R, Ho CY, Ashley E, et al. Clinical phenotype and outcome of hypertrophic cardiomyopathy associated with thin-filament gene mutations. J Am Coll Cardiol 2014;64:2589–600.

28. Tardiff JC, Hewett TE, Palmer BM, et al. Cardiac troponin T mutations result in allele-specific phenotypes in a mouse model for hypertrophic cardiomyopathy. J Clin Invest 1999;104:469–81.

29. Dorn GW. Tension-time integrals and genetic cardiomyopathy: the force is with you. Cell 2016; 165:1049–50.

30. Flenner F, Geertz B, Reischmann-Düsener S, et al. Diltiazem prevents stress-induced contractile deficits in cardiomyocytes, but does not reverse the cardiomyopathy phenotype in Mybpc3-knock-in mice. J Physiol 2017;595: 3987–99.

31. Flenner F, Friedrich FW, Ungeheuer N, et al. Ranolazine antagonizes catecholamine-induced dysfunction in isolated cardiomyocytes, but lacks long-term therapeutic effects in vivo in a mouse model of hypertrophic cardiomyopathy. Cardiovasc Res 2016;109:90–102.

32. Friedrich FW, Sotoud H, Geertz B, et al. I-1-deficiency negatively impacts survival in a cardiomyopathy mouse model. Int J Cardiol Hear Vasc 2015;8:87–94.

33. Brower GL, Gardner JD, Forman MF, et al. The relationship between myocardial extracellular matrix remodeling and ventricular function. Eur J Cardio-Thoracic Surg 2006;30:604–10.

34. Factor SM, Butany J, Sole MJ, Wigle ED, Williams WC, Rojkind M. Pathologic fibrosis and matrix connective tissue in the subaortic myocardium of patients with hypertrophic cardiomyopathy. J Am Coll Cardiol 1991;17:1343–51.

35. Shirani J, Pick R, Roberts WC, Maron BJ. Morphology and significance of the left ventricular collagen network in young patients with hypertrophic cardiomyopathy and sudden cardiac death. J Am Coll Cardiol 2000;35:36–44.

36. Lombardi R, Betocchi S, Losi MA, et al. myocardial collagen turnover in hypertrophic cardiomyopathy. Circulation 2003;108:1455–60.

37. Gershlak JR, Resnikoff JIN, Sullivan KE, Williams C, Wang RM, Black LD. Mesenchymal stem cells ability to generate traction stress in response to substrate stiffness is modulated by the changing extracellular matrix composition of the heart during development. Biochem Biophys Res Commun 2013;439:161–6.

38. Jacot JG, McCulloch AD, Omens JH. Substrate stiffness affects the functional maturation of neonatal rat ventricular myocytes. Biophys J 2008;95:3479–87.

39. Spencer CI, Baba S, Nakamura K, et al. Calcium transients closely reflect prolonged action potentials in iPSC models of inherited cardiac arrhythmia. Stem Cell Reports 2014;3:269–81.

40. Wang L, Kim K, Parikh S, et al. Hypertrophic cardiomyopathy-linked mutation in troponin T causes myofibrillar disarray and pro-arrhythmic action potential changes in human iPSC cardiomyocytes. J Mol Cell Cardiol 2018;114:320–7.

41. Wang L, Kryshtal DO, Kim K, et al. Myofilament calcium-buffering dependent action potential triangulation in human-induced pluripotent stem cell model of hypertrophic cardiomyopathy. J Am Coll Cardiol 2017;70:2600–2.

42. Landstrom AP, Dobrev D, Wehrens XHT. Calcium signaling and cardiac arrhythmias. Circ Res 2017;120:1969–93.

43. Hazeltine LB, Simmons CS, Salick MR, et al. Effects of substrate mechanics on contractility of cardiomyocytes generated from human pluripotent stem cells. Int J Cell Biol 2012;2012:1–13.

44. Rodriguez AG, Han SJ, Regnier M, Sniadecki NJ. Substrate stiffness increases twitch power of neonatal cardiomyocytes in correlation with changes in myofibril structure and intracellular calcium. Biophys J 2011;101:2455–64.

45. Ribeiro AJS, Ang YS, Fu JD, et al. Contractility of single cardiomyocytes differentiated from pluripotent stem cells depends on physiological shape and substrate stiffness. Proc Natl Acad Sci 2015;112:12705–10.

46. Boothe SD, Myers JD, Pok S, et al. The effect of substrate stiffness on cardiomyocyte action potentials. Cell Biochem Biophys 2016;74:527–35.

47. van Deel ED, Najafi A, Fontoura D, et al. In vitro model to study the effects of matrix stiffening on Ca2+ handling and myofilament function in isolated adult rat cardiomyocytes. J Physiol 2017;595:4597–610.

48. Milani-Nejad N, Canan BD, Elnakish MT, et al. The Frank-Starling mechanism involves deceleration of cross-bridge kinetics and is preserved in failing human right ventricular myocardium. Am J Physiol Heart Circ Physiol 2015;309:H2077–86.

49. Chung JH, Martin BL, Canan BD, et al. Etiology-dependent impairment of relaxation kinetics in right ventricular end-stage failing human myocardium. J Mol Cell Cardiol 2018;121:81–93.

KEY WORDS diastolic dysfunction, engineered heart tissue, fibrosis, hypertrophic cardiomyopathy, iPSC-derived cardiomyocyte, MYH7 mutation

APPENDIX For a supplemental table and figures, please see the online version of this paper.